General Disclaimer

One or more of the Following Statements may affect this Document

- This document has been reproduced from the best copy furnished by the organizational source. It is being released in the interest of making available as much information as possible.

- This document may contain data, which exceeds the sheet parameters. It was furnished in this condition by the organizational source and is the best copy available.

- This document may contain tone-on-tone or color graphs, charts and/or pictures, which have been reproduced in black and white.

- This document is paginated as submitted by the original source.

- Portions of this document are not fully legible due to the historical nature of some of the material. However, it is the best reproduction available from the original submission.

NASA Technical Memorandum 82994

Utilizing Numerical Techniques in Turbofan Inlet Acoustic Suppressor Design

Kenneth J. Baumeister
Lewis Research Center
Cleveland, Ohio

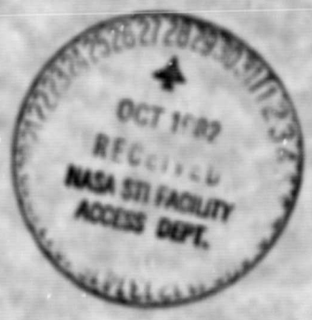

Prepared for the
Nineteenth Annual Meeting of the Society of Engineering Science
Rolla, Missouri, October 27-29, 1982

NASA

UTILIZING NUMERICAL TECHNIQUES IN TURBOFAN INLET ACOUSTIC SUPPRESSOR DESIGN

by Kenneth J. Baumeister

National Aeronautic and Space Administration

Lewis Research Center

Cleveland, Ohio 44135

E-1427

SUMMARY

Numerical theories in conjunction with previously published analytical results are used to augment current analytical theories in the acoustic design of a turbofan inlet nacelle. In particular, a newly developed finite element-integral theory is used to study the effect of the inlet lip radius on the far field radiation pattern and to determine the optimum impedance in an actual engine environment. For some single mode JT15D data, the numerical theory and experiment are found to be in a good agreement.

NOMENCLATURE

$A_{1,2,..}$	flow coefficients
C	velocity of sound normalized to the stagnation speed of sound C_o^*
C_o^*	stagnation speed of sound, m/sec
d_o^*	internal duct diameter, m
F	function equation, see Eq. (2)
H	dimensionless thickness of nacelle wall, H^*/d_o^*
H*	thickness of nacelle wall, m, see Fig. 4
i	$\sqrt{-1}$
k	wave number, ω/c
$\overline{M}$	average engine Mach number

M_o	far field Mach number, see inserts of Figs. 4 and 5
m	spinning mode number, see Eq. (1)
n	higher order radial mode number
p	pressure normalized by $\rho_o^* C_o^{*2}$
R	far field position (distance from exit plane centerline) normalized by d_o^*
r	radial coordinate normalized by duct diameter d_o^*
r_o^*	$d_o^*/2.$
t	time normalized by d_o^*/C_o^*
Z	specific acoustic impedance, normalized by $\rho_o^* C_o^*$
	$Z = \theta_r + i\chi$
z	axial coordinate normalized by d_o^*
α	angle from inlet, see Fig. 2
θ	angular coordinate
θ_r	specific acoustic resistance
ρ	density normalized by ρ_o^*
ρ_o^*	stagnation density, kg/m^3
Φ	general flow potential normalized by $C_o^* d_o^*$
ϕ	acoustic flow potential
$\bar{\phi}$	mean flow potential
χ	specific acoustic reactance
ω	angular frequency normalized by C_o^*/d_o^*

Superscripts

$\bar{}$	mean value
*	dimensional quantity

Subscripts

n	normal derivative
s	surface derivative
r,θ,z	derivatives

INTRODUCTION

Acoustically treated surfaces inside turbojet engine nacelles are commonly used to meet current aircraft noise regulations. A complete design of a turbojet acoustic suppressor (Ref. 1) requires both an estimate of the fan noise spectrum and the desired far field noise level from which a target attenuation spectrum can be determined. To obtain the desired attenuation, closed form solutions of the acoustic wave equation are commonly employed to determine the required soft wall impedance of the liner. From parametric solutions of the wave equation, Rice (Refs. 2 and 3), for example, has developed a design procedure based on mode cut-off ratio which can be conveniently and quickly used in a liner design.

By their very nature, however, closed form analytical theories require considerable simplification in the nacelle geometry and mean flow fields. For example, the optimum impedances (max attenuation) in Refs. 1 to 3 were determined for a semi-infinite uniform walled duct. However, finite element theories (Refs. 4 and 5) have been developed for the design of acoustically treated ducts which can account for the geometric complexities involved with a turbofan engine.

At the present time, numerical theories are too costly and frequency limited to perform a complete suppressor analysis. Herein, emphasis will be placed on how the numerical techniques can modify the closed form analytical results to account for complexities in the inlet which cannot be accounted

for by the closed form theories. In particular, a newly developed program (Ref. 6) is used herein to:

(1) Estimate the effect of the inlet lip radius on the far field radiation pattern and compare the results with the sharp walled Wiener-Hopf theory.

(2) Determine the effectiveness of a soft walled liner in an engine environment.

(3) Determine the optimum impedance of a liner in an engine environment.

Data comparisons will be included with the above.

FINITE ELEMENT THEORY

To predict the sound field radiated from a turbofan inlet, a variety of numerical duct acoustic programs could be employed as cited in the bibliographies of Refs. 4 and 5. At the present time, however, a finite element-integral program described in Ref. 6 is the only published program capable of simultaneously solving for both the internal and external acoustic fields of a turbojet engine. In addition, the validity of this program was established in reference 7 for the field measurements of JT15D turbofan inlet noise. Consequently, this program will be used herein.

In the finite element-integral program, the velocity potential formulation for the mean flow equations as well as the acoustic equations is employed. The velocity potential form of the governing equations was chosen since it reduced the number of dependent variables to one-third and therefore cut the computer storage and running time by an order of magnitude compared to the more general linearized gas dynamic formulation. On the other hand, when rotational flow exists in the inlet (wall and certerbody boundary layers), the potential flow cannot be used to estimate the effects of shear

(Ref. 8). However, since the flow into an inlet is reasonably modelled by potential flow and since boundary layers are small, the acoustic velocity potential is ideally suited for acoustic inlet calculations. Once the acoustic potential is determined, the acoustic pressures and velocities can be directly calculated (Ref. 6).

To obtain the acoustic equations for the inlet, first the flow potential Φ is rewritten as the sume of a steady axisymmetric mean flow potential $\bar{\phi}(r,z)$ and an acoustic potential $\phi(r,z)$ defined as

$$\Phi = \bar{\phi} + \phi(r,z)\, e^{i(\omega t - m\theta)} \tag{1}$$

To account for spinning modes, the acoustic potential in equation (1) has been modified to include $e^{im\theta}$. Also, the solutions have been assumed to be harmonic ($e^{-i\omega t}$) in time.

The program first calculates the mean flow distribution for the inlet. The mean flow quantities, $\bar{\phi}$, are independent of time and thereby satisfy the usual steady mean flow equation. Next, the mean flow solution is put into the potential acoustic wave equation, which is of the form.

$$F(\phi) = A_1\phi_{rr} + A_2\phi_{zz} + A_3\phi_{rz} + A_4\phi_r + A_5\phi_z + A_6\phi = 0 \tag{2}$$

where the A's contain all the mean flow quantities and are derived in Ref. 6.

To solve the acoustic wave equation (2), the sound field is divided into two regions: the sound field within and near the inlet which is computed using the finite element method and the radiation field beyond the inlet which is calculated using an integral solution technique (Ref. 9). Numerical iteration between the interior and exterior regions is required to obtain a continuous acoustic field across the interface. The iteration procedure between the two regions requires the acoustic potential and impedance to be identical on either side of the boundary.

As seen in Fig. 1, the interior portion of a test JT15D inlet has been

divided into a number of triangular Hermitian elements. For clarity, the number of elements shown have been greatly reduced from the actual number used. The Hermitian formulation enforces continuity of both the velocity potential and its derivatives at the nodes, thereby reducing the number of elements required to accurately predict the sound field.

Along the nacelle wall, the boundary condition at the surface of a locally reacting sound absorbent soft-wall duct can be expressed in terms of a specific acoustic impedance Z:

$$Z = \theta_r + i\chi \tag{3}$$

where θ_r is the specific acoustic resistance and χ the specific acoustic reactance. Majjigi (Ref. 10) has shown that a proper formulation of the requirement of continuity of particle displacement yields

$$\phi_n = \frac{-p}{Z} - \frac{1}{i\omega}\bar{\phi}_s \frac{\partial}{\partial s}\left(\frac{p}{Z}\right) + \frac{p}{i\omega Z}\bar{\phi}_{nn} \tag{4}$$

where the pressure p is defined by

$$p = -\bar{\rho}\,(i\omega\phi + \bar{\phi}_z\phi_z + \bar{\phi}_r\phi). \tag{5}$$

In this analysis, it is assumed that the last term in equation (4) is negligible since ϕ_{nn} is quite small (Ref. 6).

In the integral technique applied in the external field, the Green's theorem is used to transform the wave equation into an equivalent problem of solving an integral equation over the boundary of the region designated by asterisks (*) as shown in figure 1. The integral technique can only be applied in cases where the properties of the medium are constant or the differential equation describing the medium can be transformed into a constant property problem. Consequently, the interface separating the interior (finite element) and exterior regions must be extended sufficiently far from the exit so that the flow is approximately uniform.

For the uniform flow, equation (2) reduces to

$$F(\phi) = \phi_{rr} + \phi_{r/r} + [1 - M_o^2]\phi_{zz} + \left(k^2 - \frac{m^2}{r^2}\right)\phi + 2ikM_o\phi_z = 0 \qquad (6)$$

In Ref, 9, Meyer et al have transformed euqation (6) along with the Sommerfield radiation boundary conditions into the integral form. The Meyer et al approach was used. The accuracy of their results has been previously demonstrated.

At the interface between the interior and exterior regions, the initial impedance is chosen to be $\rho_o^* C_o^*$. As mentioned earlier, to determine the exact value of the exit impedance as well as the acoustic velocity and pressure, a simple iteration procedure based on the method of successive substitution has been used. The exact formulation is detailed in Ref. 6.

STATIC TEST DATA

The finite element-integral program will be employed in evaluating various aspects of a turbofan engine acoustic design. Some theoretical comparisons will be made with previously published data. In particular, both hard and soft wall JT15D engine acoustic data are available in Ref. 12. The acoustic tests outlined in Ref. 12 were performed at the NASA Lewis Vertical Lift Facility. The experiments documented in Ref. 12 are extremely useful because only one acoustic mode was made to dominate the noise spectrum. A tabular summary of some of the data used in Ref. 12 can be found in Ref. 7. As documented in Ref. 12, a spool piece with 41 equally spaced radial rods was attached to the engine front flange. These rods extended 6.4 cm (2.5 inches) from the outer nacelle wall into the inlet flow field. The wakes of these rods interact with the 28 fan blades to produce a blade passage frequency (BPF) tone with 13 circumferential lobes. Data were taken at a

fan speed of 6750 rpm with an average inlet Mach number of 0.147. In this case, only the lowest radial mode can propagate. Thus, the usual problems of separation of acoustic modes and contamination by noise floors are to a large extent eliminated in the data reduction.

NUMERICAL RESULTS

The finite element-integral program will now be used to evaluate the effect of inlet wall thickness and soft walls on the performance of turbofan inlets, and to compare the results with the simpler closed form theories. In particular, the finite element-integral program is now applied to the JT15D engine experiment of Ref. 12 to determine the far field radiation pattern and suppressor effectiveness. The approximate dimensions of the JT15D inlet shown in Fig. 1 are presented in the insert of Fig. 2. For numerical calculations, the exact dimensions of the nacelle can be found in Ref. 7.

For the calculations reported in the paper, the finite element computer code subdivided the interior region of the inlet into 320 Hermitian elements. These elements used 1003 nodal points of which 683 are triangular vertices with 2049 degrees of freedom (ϕ, ϕ_r, ϕ_z unknowns) and 320 centroid unknowns for a total of 2369 unknowns. The computer code for the integral technique subdivided the interface into 59 segments.

Wall Thickness Effects

The calculated far field radiation pattern for the (13,0) mode at 3150 Hz (BPF at 6750 rpm) is shown in Fig. 2 at 24.4 m and 5.42 m from the inlet. The similarity between the two far field distributions indicates that near field effects are absent.

For the noise source at the fan plane, both the radial pressure distribution of the (13,0) mode and a uniform radial pressure distribution in the

annulus were used. Since all higher order radials (13,n) are cut off, and only the (13,0) mode propagates the far field pressure distribution had the identical shape when the far field SPL level was normalized to a common value of 100 dB at 60 degrees. The jump at 30° in Fig. 2 is not real and results from selecting insufficient number of elements. Fewer elements produced a larger jump. The average inlet Mach number ahead of the spinner is 0.147.

The numerical results are replotted in Fig. 3 along with the Savkar (Ref. 13) Wiener-Hopf solution for a sharp edge. Savkar's theory was modified for convection effects using a velocity correction factor from Ref. (14) (Eq. (8)). Also, the experimental data from Ref. 12 for the JT15D engine with inlet rods are shown.

As seen in Fig. 3, the experimental data for the thick bellmouth inlet are in good agreement with the finite element analysis. The peaks in the data and analysis, however, are about 10 degrees apart. Also, as seen in Fig. 3, the sharp-lip Wiener-Hopf analytical solution predicts much more acoustic radiation propagating to higher angles than either the data or the finite element solution. Apparently, the thick bellmouth flight inlet shields the acoustic radiation from the higher angles. For a thick wall inlet, therefore, the simpler analytical theories are not sufficient. Some type of numerical theory or design empirical rule must be employed.

To assess the effect of the nacelle shape, finite element calculations were run with three distinct values of lip radius. For zero Mach number (no mean flow), the effect of the nacelle lip thickness on the narrow band tone directivity pattern is shown in Fig. 4. At the higher angles, the inlet lip has produced 10 dB level changes. The inlet with H = 0.1 is very nearly identical to the Wiener-Hopf solution shown in Fig. 3.

In the next calculation, the mean flow was "turned on" to the average Mach number of 0.147 associated with the experimental data plotted in Fig. 3. Again, the effect of the nacelle lip thickness on the narrow band tone directivity pattern is shown in Fig. 5. As seen by a comparison between Figs. 4 and 5, very little change occurs in the SPL directionality pattern for H of 0.1 and 0.25. A slight upward shift in the H = 0.5 curve is seen. Overall, flow gradients had minor effects on the directivity pattern. Apparently, the low Mach number associated with this data is insufficient to cause significant refraction effects.

Finally, the narrow band tone directivity with a flight type inlet nacelle mounted on a JT15D engine is shown in Fig. 6. Again, the average inlet Mach number is 0.147. Also shown in Fig. 6 are the Wiener-Hopf solution for a sharp thin inlet and the thick wall inlet solution both of Fig. 3. A comparison of the various curves in Fig. 6 indicates that the Wiener-Hopf analytical solution will probably perform adequately for flight inlets at least for low duct Mach number. Some minor differences occur between the flight inlet and Wiener-Hopf solutions for angles greater than 90 degrees.

Soft Wall Attenuation

In a turbofan suppressor design, an analytical program will often specify a wall impedance and present a predicted sound power attenuation. As an additional design aid, the numerical program can now evaluate the performance of the suppressor in a simulated engine environment which includes complications arising from both the mean flow field and the inlet geometry.

In the experiments of Ref. 12, three suppressor designs were built having estimated nominal values of resistance of 2.272, 1.136, and 0.638 (Table 1, Ref. 12). The suppressors were all specially built to each have an identical reactance of 0.5 which is stiffness controlled at 3150 Hz. The

finite element-integral method is now used to evaluate the performance of these suppressors in the simulated turbofan engine environment. A comparison with the experimental data will also be made.

For a soft walled suppressor, the sound attenuation of the liner can be determined numerically by the insertion loss method. First, the far field SPL level is determined for the hard wall nacelle, such as shown in Fig. 2. Next, the appropriate impedance boundary conditions are inserted between the nodes which correspond exactly to the entrance and exit of the active liner. For the JT15D inlet under consideration, nodes 18 and 44 in Fig. 1 bounded the soft wall section of the nacelle. Finally, the far field radiation pattern is again calculated with the soft walled boundary condition included.

Fig. 7 displays the calculated far field radiation pattern for the same fan source as in Fig. 2 but with a soft wall suppressor of $L/d_o = .15$ having a resistance of 0.638 and a reactance of 0.5. A comparison of Fig. 2 with Fig. 7 shows the sound radiation pattern has the same far field shape but is decreased in magnitude by about 22 dB for all angles. This attenuation along with calculated attenuations for other resistance values are plotted in Fig. 8. Again, for a single mode, the attenuations is the far field are independent of the angle from the inlet so only one curve is shown in Fig. 8.

In Fig. 8, a comparison with the experimental data is also made for data between 50 and 80 degrees. These angles were chosen since in the experiment the sound pressure level for these angles stood well above the broadband noise floor. As seen in Fig. 8, the experiment and theory are in good agreement. The two to three dB scatter in the data results from the natural consequences of running a full-scale engine over a long period of time under varying environmental conditions.

Clearly, Fig. 8 establishes the validity of using a numerical theory to predict the actual performance of a liner to an engine environment.

Optimum Wall Impedance

In addition to the effects of the nacelle lip and the performance of individual suppressors, optimizing the noise suppressor for maximum attenuation is also extremely important in the design of an acoustic nacelle. The maximum possible attenuation occurs at the so-called optimum impedance. For a particular mode or more generally for modes with common cut-off ;s, the optimum impedance can be determined analytically from semi-infinite duct theory using a singe soft wall mode (Ref. 3) Again, it is desirable to account for the actual engine environment is the determination of the optimum impedance.

For the m = 13 zeroth radial order mode associated with the suppressor data of Ref. 12, the single mode optimum impedance was calculated to be 1.136 + 0.5i where 1.136 represents the specific resistance θ_r of the wall impedance while the 0.5 represents the specific reactance χ which is stiffness controlled at 3150 Hz. The maximum attenuation for this liner was determined from single mode duct theory to be approximately 200 dB per L/d_o or 30 dB for an L/d_o of 0.15.

The theoretical optimum impedance can now be determined for the actual JT15D inlet geometry, flow field, and finite length liner. Most likely, large amounts of computer time would be required to fully numerically determine the optimum impedance in an actual turbofan installation. However, the basic idea of the present paper is to utilize the numerical theory to fine-tune the more convenient analytical theories. Consequently, the analytical theories are first used as a starting point in a numerical search for the actual installation optimum.

Rice (Refs. 2 and 3) has comprehensively correlated the optimum impedance for individual modes for a wide range of acoustic and mean flow parameters. Consequently, this optimum impedance represents a convenient starting point in the numerical search for the actual optimum impedance in the turbofan nacelle.

Generally, as shown by Unruh (Refs. 15 and 16), the optimum resistance for a finite length liner will be lower than the single mode value due to the generation of higher order modes. Individually, the higher order modes have lower optimum impedance (Ref. 2). Modal scattering is extremely importance for a single mode entering a very short acoustic liner such as used in the experiments of Ref. 12 ($L/d_0 = 0.15$). The impedance discontinuity causes the single hard wall mode to scatter into several radial modes in the soft wall section. Since the liner is quite short the higher radial modes contribute significantly to the overall suppression. This effect is very pronounced at low frequencies (Ref. 15) and, as shown herein, for higher order modes which have relatively long axial wave lengths (similar to low frequency sound propagation).

Starting with the single mode optimum impedance (solid circle in Fig. 9), using common optimization techniques (Ref. 17), and initially directing the search towards lower values of resistance, the optimum impedance can be quickly determined. In this case, the optimum impedance is lowered to $0.62 + i\,0.9$. Also, as seen in Fig. 9, the finite element calculation for the actual installation yields a maximum possible attentuation of 50 dB compared to the 30 dB predicted by the single mode theory. This is to be expected since the higher order modes have higher attenuation coefficients.

Finite liner length, flow gradients, and nacelle geometry can all contribute to the 20 dB enhanced calculated attenuation for the actual nacelle

geometry over the calculated value from duct theory which considered only a single soft wall mode. Unfortunately, the individual contributions to the attenuation cannot be explicity determined.

At the single mode optimum impedance of 1.136 + i0.5, the attenuation for the L/d_0 of 0.15 duct is shown in Fig. 9 to be 30 dB while the finite element value is 17 dB. To illustrate the sensitivity of L/d_0 effects, an assessment of suppressor length on attenuation at this fixed impedance can be made. As the acoustic liner is lengthened (smaller d_0/L, the numerical calculated attentuation approaches the single mode attenuation shown at $d_0/L = 0$. Therefore, a significant portion of the attenuation enhancement can be attributed to modal scattering effects. For an extremely long duct, the lowest order propagating mode would completely dominate the sound attenuation.

CONCLUSIONS

Numerical theories are shown to be versatile aids in the design of acoustic nacelles for turbofan engines. The numerical analysis can account for complications arising from variations in the mean flow field and inlet geometry. Example problems show that inlet lip effects and finite liner lengths can significantly effect the acoustic characteristics of an inlet.

REFERENCES

1. Minner, G. L.; and Rice, E. J.: Computer Method for Design of Acoustic Liners for Turbofan Engines. NASA TM X-3317, Oct. 1976.
2. Rice, E. J.: Optimum Wall Impedance for Spinning Modes - A Correlation with Mode Cut-Off Ration. Aircr., vol. 16, no. 5, May 1979, pp. 336-343.

3. Rice, E. J.: Modal Propagation Angles in Ducts with Soft Walls and their Connection with Suppressor Performance. NASA TM-79081, Mar. 1979.

4. Baumeister, K. J.: Numerical Techniques in Linear Duct Acoustics - A Status Report. Ind., vol. 103, no. 3, Aug. 1981, pp. 270-281.

5. Baumeister, K. J.: Numerical Techniques in Linear Duct Acoustics - 1980-81 Update. NASA TM-82730, Nov. 1981.

6. Horowitz, S. J.; Sigman, R. K.; and Zinn, B. T.: An Iterative Finite Element-Integral Technique for Predicting Sound Radiation from Turbofan Inlets in Steady Flight. AIAA Paper 82-0124, Jan. 1982.

7. Baumeister, K. J.; and Horowitz, S. J.: Finite Element-Integral Simulation of Static and Flight Fan Noise Radiation from the JT15D Turbofan Engine. NASA TM-82936, Aug. 1982.

8. Baumeister, K. J.; and Majjigi, R. K.: Applications of Velocity Potential Function to Acoustic Duct Propagation Using Finite Elements. AIAA, vol. 18, no. 5, May 1980, pp. 509-514.

9. Meyer, W. L.; Et al.: Prediction of the Sound Field Radiated from Axisymmetric Surfaces. Am., vol. 65, no. 3, Mar. 1979, pp. 631-638.

10. Majjigi, R. K.: Application of Finite Element Techniques in Predicting the Acoustic Properties of Turbofan Inlets. Ph.D. Thesis, Georgia Inst. of Tech., 1979.

11. Tester, B. J.: The Propagation and Attenuation of Sound in Lined Ducts Containing Uniform or 'Plug' Flow. Sound, vol. 28, no. 2, May 1973, pp. 151-203.

12. Heidelberg, L. J.; Rice, E. J.; and Homyak, L.: Acoustic Performance of Inlet Suppressors on an Engine Generating a Single Mode. AIAA Paper 81-1965, 1981.

13. Savkar, S. D.: Radiation of Cylindrical Duct Acoustic Modes with Flow Mismatch, Sound, vol. 42, no. 3, Oct. 1975, pp. 363-386.

14. Heidmann, M. F.; Saule, A. V.; and McArdle, J. G.: Predicted and Observed Modal Radiation Patterns from JT15D Engine with Inlet Rods. Aircr., vol. 17, no. 7, July 1980, pp. 493-499.

15. Inruh, J. F.: Finite Length Tuning for Low Frequency Lining Design. Sound, vol. 45, no. 1, 1976, pp. 5-14.

16. Unruh, J. F.; and Price, I. R.: Experimental Verification of a Finite Length Tuning Concept for Acoustic Lining Design. Sound Vib., vol. 49, no. 3, Dec. 1976, pp. 393-402.

17. Kuester, J. L.; and Mize, J. H.: Optimization Techniques with Fortran. McGraw-Hill Book Company, 1973.

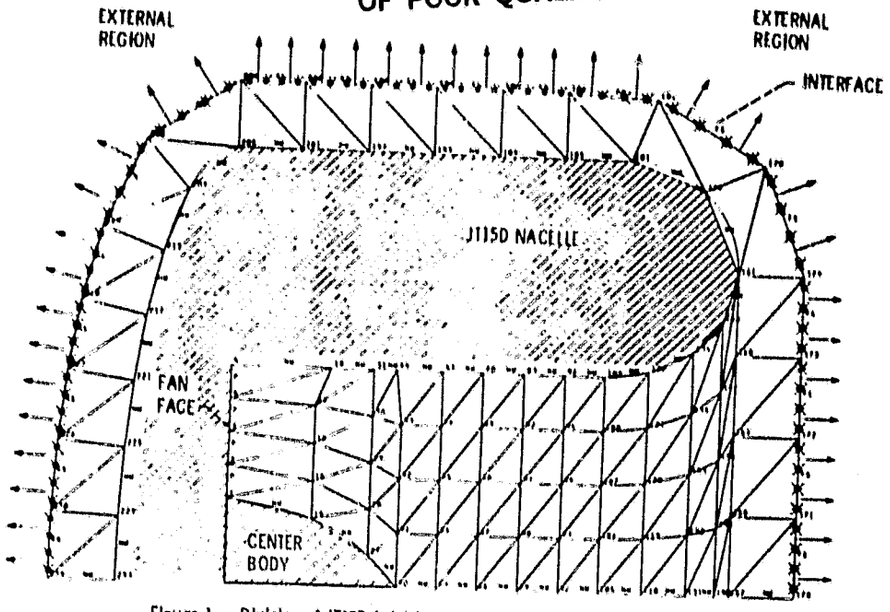

Figure 1. - Division of JT15D inlet into Hermitian triangular elements.

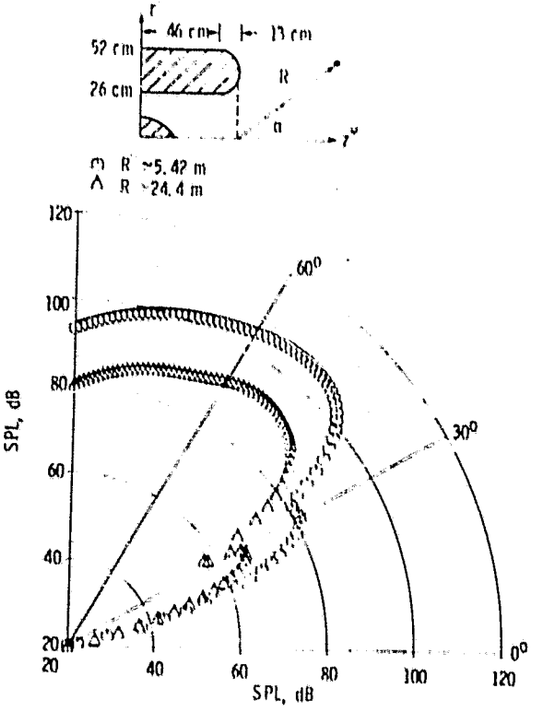

Figure 2. - Theoretical far field SPL directionality pattern for 3150 Hz and (13, 0) mode at source for hard wall configuration.

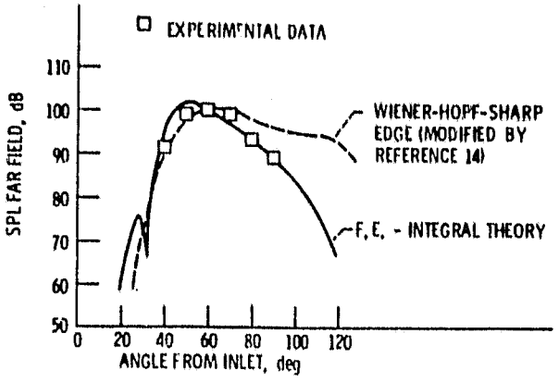

Figure 3. - Comparison of theory and experiment for narrow band tone directivity pattern at 3150 Hz and (13, 0) mode for hard wall configuration (theory and data normalized to 100 dB at 60 deg).

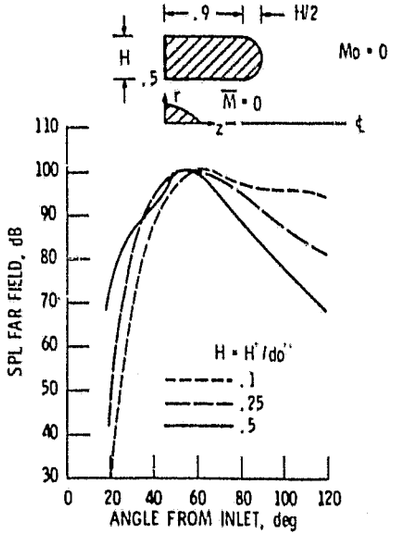

Figure 4. - Effect of nacelle lip thickness on narrow band tone directivity pattern for $\bar{M} = 0$ at 3150 Hz and (13, 0) mode for hard wall configuration (theory normalized to 100 dB at 60 deg.

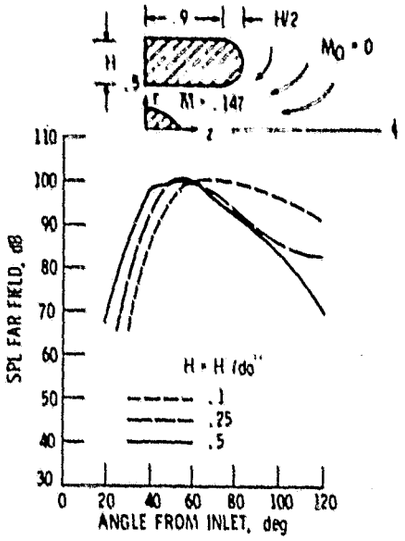

Figure 5. - Effect of nacelle lip thickness on narrow band tone directivity pattern for $\bar{M}$ = .147 and M_0 = 0 at 3150 Hz and (13, 0) mode for hard wall configuration (theory normalized to 100 dB at 60 deg).

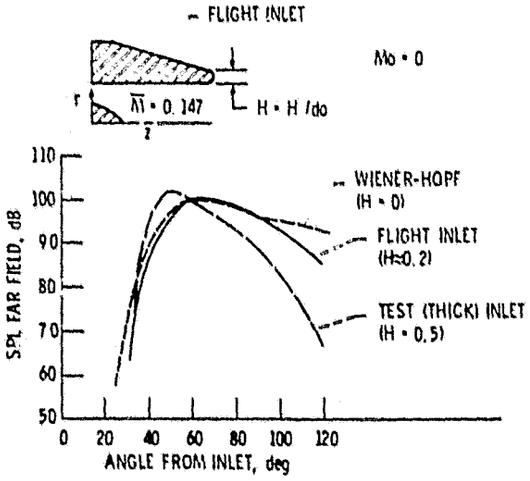

Figure 6. - Comparison of inlet shape on narrow band tone directivity pattern at 3150 Hz and (13, 0) mode for hard wall configuration (normalized to 100 dB at 60 deg).

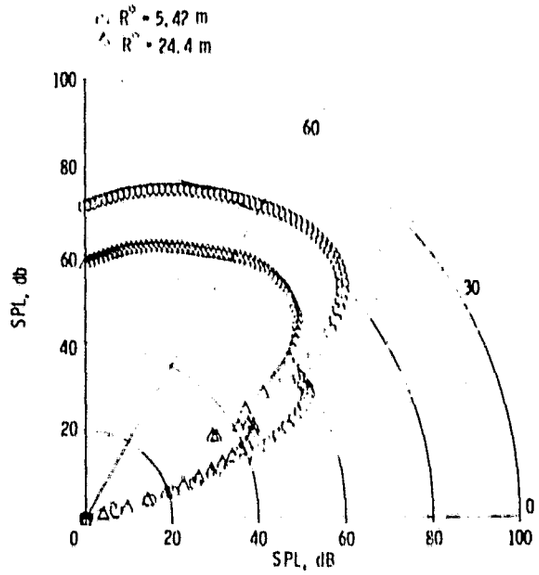

Figure 7. - Theoretical far field SPL directionality pattern for 3150 Hz and (13, 0) mode at source for soft wall configuration (θ = 0.638, χ = 0.5)

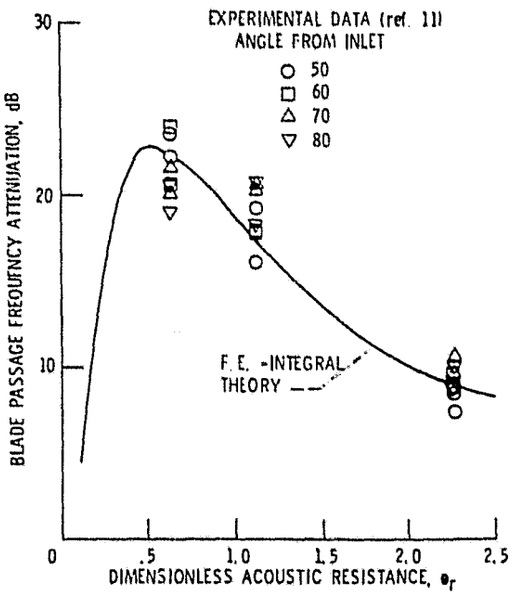

Figure 8. - Comparison of data with theoretical attenuation as a function of resistance for the (13, 0) mode at 3150 Hz (reactance X = .5) between 50-80 deg from inlet center line.

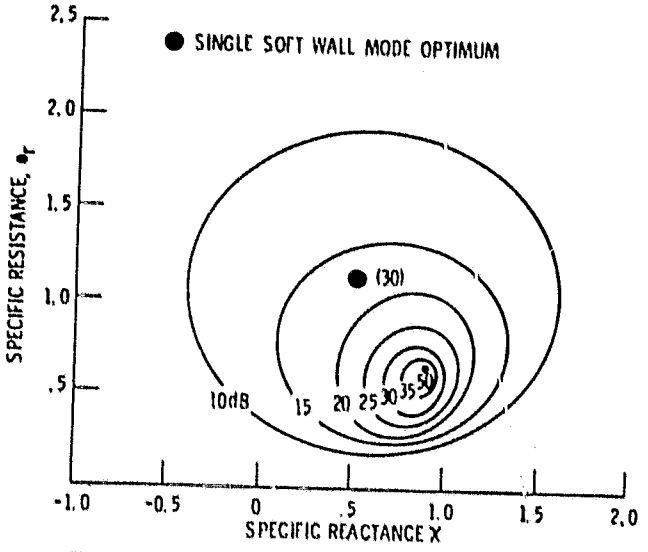

Figure 9 - Sound power attenuation contours at 3150 Hz for (13, 0) mode with a liner L/do of 15

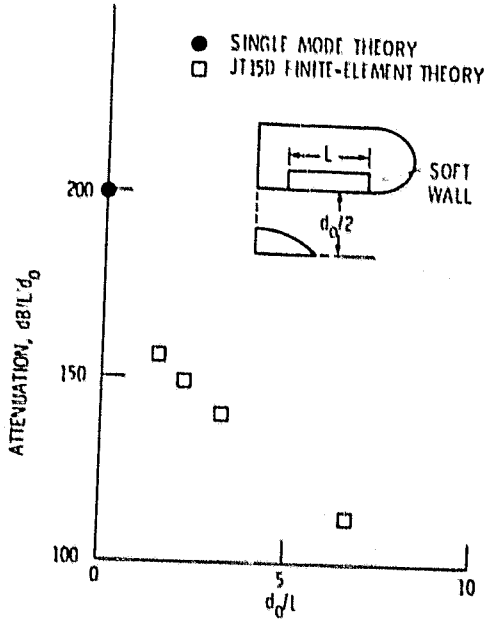

Figure 10. - Effect of liner length on normalized total liner attenuation for θ_r = 1.136 and X = 0.5.